Int J Adv Manuf Technol (2016) 86:2339–2351
DOI 10.1007/s00170-016-8358-1

ORIGINAL ARTICLE

# Influence of weld geometry and process parameters on the quality of underwater wet friction taper plug welding

**Shengli Li**[1] · **Xinqi Yang**[1] · **Lei Cui**[1] · **Yayun Yin**[1]

Received: 29 September 2015 / Accepted: 13 January 2016 / Published online: 26 January 2016


**Abstract** In the present study, a number of joints were fabricated successfully on DH36 marine steel sheet in underwater wet based on friction taper plug welding (FTPW). The influences of the plug and hole geometry parameters combination on the quality of welded joint forming were first investigated. It was found that tapered holes and plugs were the preferred choice and a suitable cone angle range was obtained. Using the preferred hole and plug designed further expand the range of welding parameters to explore process parameters influence on the welding quality. Bonding mechanism and microstructural evolution to FTP welds were investigated with multiple observations. Mechanical properties of the obtained joints were also evaluated with tensile and Charpy impact tests by reference to AWS D3.6 Underwater Welding Code. The best result is found as the joint welded with 7500 rpm and 40 kN which has 535.6 MPa ultimate tensile strength, 22.5 % elongation, and 42.5 J impact energy at bonding line.

**Keywords** Underwater wet welding · Friction taper plug welding · Geometry parameters · Bonding mechanism microstructures · Mechanical properties

## 1 Introduction

Underwater welding is an effective method for repairing damaged metal components and structures during construction and operation of submarine pipelines and offshore platforms [1]. However, underwater welding is more difficult in comparison to that performed at open air because of: limited visibility, higher pressure, hydrogen content in weld metal and higher cooling rates, which contribute to the formation of welding defects. These phenomena reduce the underwater weldability of higher-strength steels [1–3]. In order to solve the problems of underwater welding, researchers have been working to find better underwater welding processes in recent years. Traditional underwater welding techniques based on fusion welding can be classified as wet welding, dry welding, and local cavity welding. But experiments and engineering practices show that there are still thorny problems using underwater wet fusion welding, such as arc instability, weld porosity, hydrogen embrittlement, etc.[2, 4–6].

Friction taper plug welding (FTPW),as a new solid-state joining process derived from friction welding, was invented by The Welding Institute (TWI) in 1992 [7]. FTPW is regarded as a promising repairing technology which involves rotating a consumable plug co-axially into a blind hole drilled in advance under an applied load. Both frictional heat and axial load would perform in the process so that the plug material is softened, and as the process continues, the consumable rod is further deposited continuously in the blind hole to form a sound weld [8, 9]. This welding method enjoys great advantages as a solid-state welding, such as no defects related to fusion welding, low cost consumables, and environmentally friendly. Most importantly, FTPW process is greatly suited for automated and remote control so that it can be performed as a repair technique in deep underwater condition and other hazardous environments [7, 10].

In the FTPW process, there are four main parameters: axial force, rotating speed, burn-off, and forging force [11–13]. ROTATING SPEED refers to the rotational speed of the plug materials which produce a relative velocity at the faying surface and provide sufficient frictional heat. And rotational

✉ Lei Cui
cuileitju@163.com

[1] Tianjin Key Laboratory of Advanced Joining Technology, School of Materials Science and Engineering, Tianjin University, Tianjin 300072, People's Republic of China

speed has effects on the mechanical properties of the FTP welded joints. AXIAL FORCE means the force imposed on the plug axially and needs to be high enough to generate adequate friction force and sufficient frictional heat. Thus, the faying surface could be contacted intimately and the welding process is consecutive. BURN-OFF is the length consumption of the plug materials during welding to fill the blind hole totally. Burn-off mainly depends on the geometrical sizes of the samples. FORGING FORCE refers to the force which needs to be slightly higher than the axial force applied axially on the plug at the end of the friction welding process. Besides, the geometrical shape and dimensions of the plug and the hole are also important factors which should be considered.

Some researchers have conducted a series of investigations to explore the factors affecting quality of FTP-welded joints [11–16]. Meyer examined two different approaches to study the influence of the stud and hole shape on the quality of the weld. In the first approach, a hole with a flat bottom was selected with studs with different tip designed. In the second approach, chamfered studs and hole bottoms were used. The results indicated that the hole shape, rather than the stud geometrical dimension has a major influence in achieving bonding of the FTPW joint [11]. Hattingh et al. studied the influence of rotational speed, forging force, and burn-off on weld defects and mechanical properties in AISI 4140 steel FTSW. They found that the maximum tensile strength of FTPW joints could achieve 94 % of the parent material when low forging force, high rotational speed, and high burn-off process parameters were selected [13]. Cui et al. investigated weld performances of S355 low alloy structure steel with 6500~7500 rpm rotational speed and axial force of 20~40 kN in air conditions. It was found that defect-free welds exhibit favorable tensile properties of which 548.3 MPa ultimate tensile strength and 27.5 % maximum elongation could be reached [14]. Yin et al.

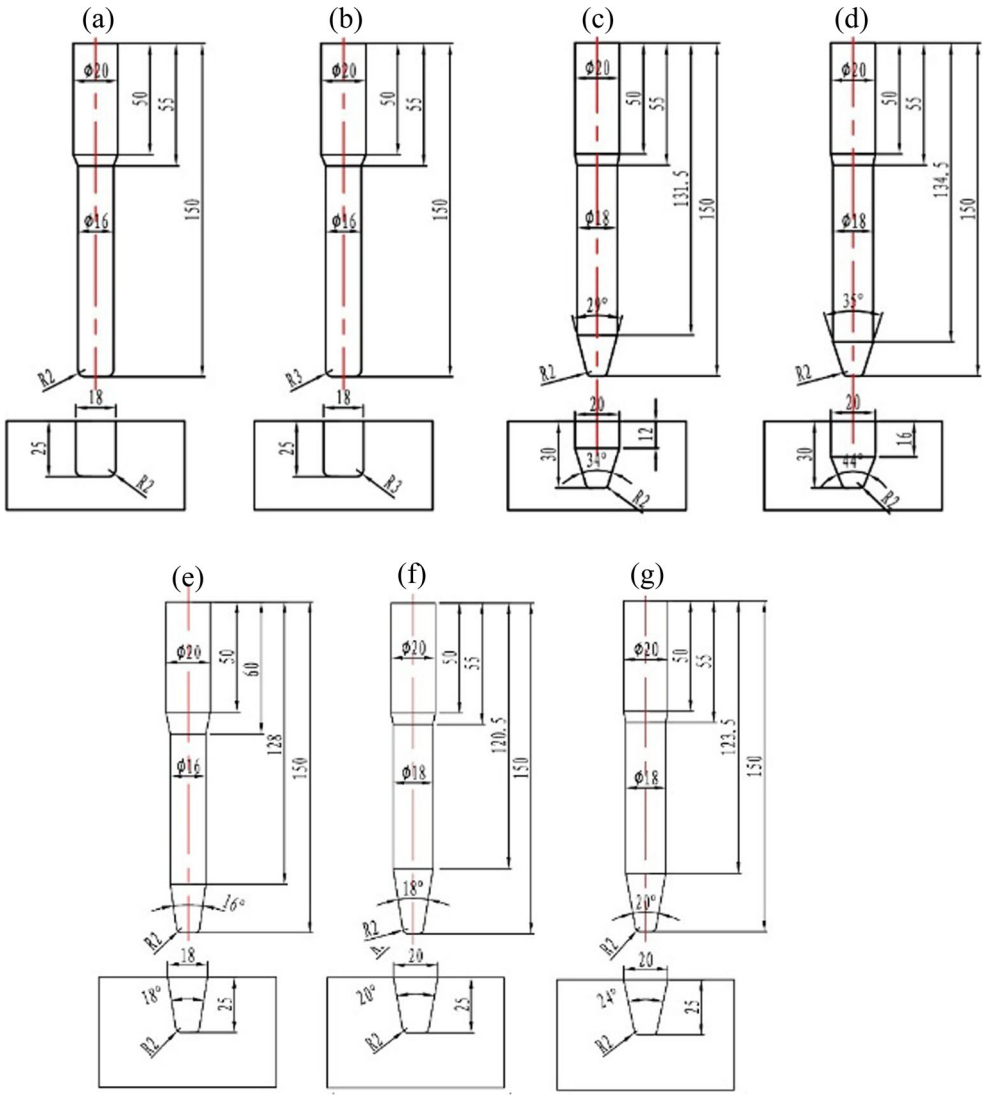


**Fig. 1** Design of the hole and plug with different geometry parameters

**Table 1** Welding parameters and sample number for investigating different geometry dimensions influence on the quality of weld forming

| Sample ID | Welding parameters | | | | |
|---|---|---|---|---|---|
| | Rotational speed (rpm) | Axial force (kN) | Forging force (kN) | Burn-off (mm) | Forging time (s) |
| A-1 (B-1/C-1/D-1/E-1/F-1/G-1) | 7000 | 25 | 30 | 15 | 10 |
| A-2 (B-2/C-2/D-2/E-2/F-2/G-2) | | 30 | 35 | | |
| A-3 (B-3/C-3/D-3/E-3/F-3/G-3) | | 35 | 40 | | |
| A-4 (B-4/C-4/D-4/E-4/F-4/G-4) | | 40 | 45 | | |

studied formation process and bonding characteristics through burn-off increasing experiment, and proposed the importance of burn-off value in achieving defect-free weld [16].

In our former study, Cui et al. explored the primary process of underwater FTPW and typical microstructures and mechanical properties of welded joints on such steels. It was found that such process could perform in underwater wet condition at 7000 rpm rotational speed and various axial force ranged in 30~50 kN. The obtained joints exhibit good bonding qualities between the hole sidewall and plug material and have no any metallurgical defects. The mechanical properties of the obtained welded joints could match the requirement of marine use [17]. However, the geometry of the plug and hole will not only directly affect the selection of welding parameters, but also influence welding defects forming. Moreover, extensive investigation in open literatures about the influence of geometrical parameters on the underwater FTP welded joints has not found. Hence, we thought that it would be very interesting and of practical importance to explore how the geometrical parameter change will affect the welding quality. Furthermore, in the present investigation, we also broadened the welding parameter settings and further discuss their influences on the weld qualities, microstructures, and mechanical properties.

## 2 Experimental procedures

The material used for the base metal and plug is normalized DH36 steel with the basic microstructure of ferrite and pearlite and the chemical composition of (wt %) 0.18 C, 0.5 Si, 0.57 Mn, 0.31 Nb. The basic properties of the steel (test value) are of 160 $HV_{10}$ hardness, 361 MPa yield strength, 531 MPa ultimate tensile strength, 23.5 % elongation, and 157 J V-notch impact energy at −20 °C. In order to investigate influence of geometrical dimensions of the blind hole and plug on the welded joint forming, seven different geometrical parameters of plug and corresponding plug hole are designed based on our initial research, which mainly include cylindrical hole and plug (type A and B), cylindrical combination tapered hole and plug (type C and D), tapered hole and plug (type E, F, and G). Details of the hole and plug are shown in Fig. 1. For facilitation analysis of the geometric shape influence, the rotational speeds were selected primarily as 7000 rpm. And, for each rotating speed, the applied axial force was in the range of 25~40 kN in steps of 5 kN. Details of the process parameters and the sample name were listed in Table 1. In order to facilitate discussion, in Table 1, the welded joints obtained from Fig. 1 marked as A~G plug and hole are respectively defined as A~G. During welding, welding peak torque also was collected for investigating the variation geometrical parameters effect on the welding torque. In particular, all welding trials were conducted under the condition that the experimental plates and welding areas were totally immerged in the water for simulating the underwater wet condition.

Then the type G plug and hole geometry combination was used to determine the welding parameters influence on the quality of FTP welded joints. Six different axial forces and three different rotational speeds were selected with this

**Table 2** Welding parameters for investigating variation welding parameters influence on the quality of weld forming

| Sample ID | Rotational speed (rpm) | Axial force (kN) | Burn-off (mm) | Forging force (kN) | Forging time (s) |
|---|---|---|---|---|---|
| A | 7500 | 25 | 15 | 30 | 10 |
| B | | 30 | | 35 | |
| C | | 35 | | 40 | |
| D | | 40 | | 45 | |
| E | | 45 | | 50 | |
| F | | 50 | | 55 | |
| G | 7000 | 25 | | 30 | |
| H | | 30 | | 35 | |
| I | | 35 | | 40 | |
| J | | 40 | | 45 | |
| K | | 45 | | 50 | |
| L | | 50 | | 55 | |
| M | 6500 | 25 | | 30 | |
| N | | 30 | | 35 | |
| O | | 35 | | 40 | |
| P | | 40 | | 45 | |
| Q | | 45 | | 50 | |
| R | | 50 | | 55 | |

**Table 3** Tensile and impact test results

| Sample ID | Defect examination | Tensile property | | | 0 °C impact energy (J) |
|---|---|---|---|---|---|
| | | $\sigma_b$ (MPa) | δ (%) | Failure location | |
| A | Defect free | 461.5 | 15.5 | BL | – |
| B | Defect free | 392.7 | 7.5 | BL | 36 ± 5.5 |
| C | Defect free | 470.8 | 14.0 | BL | 31.7 ± 3.5 |
| D | Defect free | 535.6 | 22.5 | BM | 42.5 ± 6 |
| E | Defect free | 495.2 | 14.0 | BL | 27 ± 3.5 |
| F | Defect free | 300.5 | 0.5 | BL | 15.5 ± 4 |
| G | Lack of bonding | 476.3 | 16.5 | BL | – |
| H | Defect free | 468.1 | 15 | BL | 27 ± 3 |
| I | Defect free | 523.5 | 18.5 | BL | 30.5 ± 3.5 |
| J | Defect free | 450.5 | 7.0 | BL | 15.5 ± 1.5 |
| K | Defect free | 524.1 | 16.5 | BL | 39.5 ± 8.5 |
| L | Defect free | 520.3 | 18.5 | BL | 21.5 ± 1.5 |
| M | Lack of bonding | 324.5 | 1.0 | BL | – |
| N | Lack of bonding | 355.1 | 1.5 | BL | – |
| O | Lack of bonding | 398.7 | 2.5 | BL | – |
| P | Defect free | 418.5 | 2.0 | BL | – |
| Q | Lack of bonding | 330.0 | 1.0 | BL | – |
| R | Unweldable | | | | |

geometric shape. For convenience of discussion, detailed welding parameters and samples welded successfully with the mentioned parameters are numbered A~R as illustrated in Table 2.

An OLYMPUS GX51 optical microscope (OM) was used for defect examinations and preliminary microstructural observations on the cross-sections of samples etched with 4 % nital solutions for about 15 s. Detailed examinations were conducted on the Hitachi-S4800 field emission scanning electron microscope (FE-SEM) with an electron backscattered diffraction (EBSD) system as the sample was polished with an electrolyte consisting of 650 ml alcohol, 100 ml perchloric acid, and 50 ml distilled water at 31 V for 25 s at 20 °C. Moreover, thin foils of samples were also examined by Tecnai G2F20 transmission electron microscopy (TEM). Hardness distribution ($HV_{10}$) of the FTP weld was evaluated using 432SVD Vickers hardness tester with a 20 × 20 points matrix throughout the weld on the sample welded with 7000 rpm rotating speed and 35 kN axial force. To evaluate the welding quality, tensile property (20 °C) and Charpy V-notch impact property (0 °C) were examined and then contrasted to the requirement of AWS D3.6 Underwater Welding Code [18]. Under each parameter, three standard tensile specimens and impact specimens were machined. The average value of the three test results was adopted. Details of tensile and impact samples are shown in Fig. 2a, b.

## 3 Results

### 3.1 Macro observations for different geometry parameters

Figure 3 shows type A and B plug and hole geometry obtained joints cross-sectioning macrostructures. In the case of type A

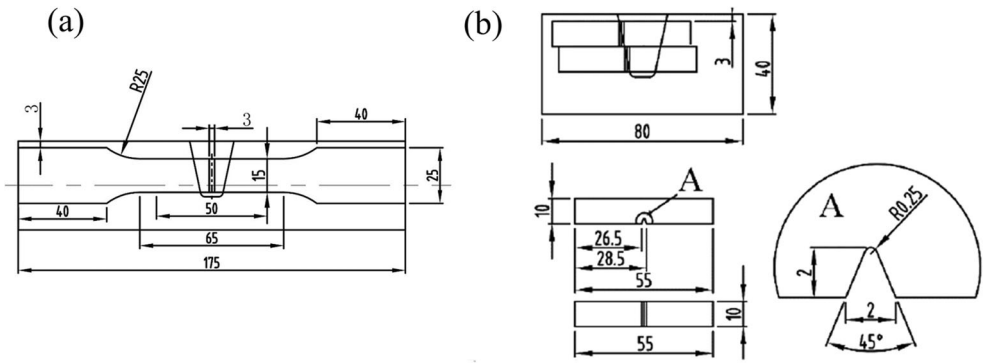


**Fig. 2** **a** Details of tensile testing specimen and **b** details of V-notched impact specimen

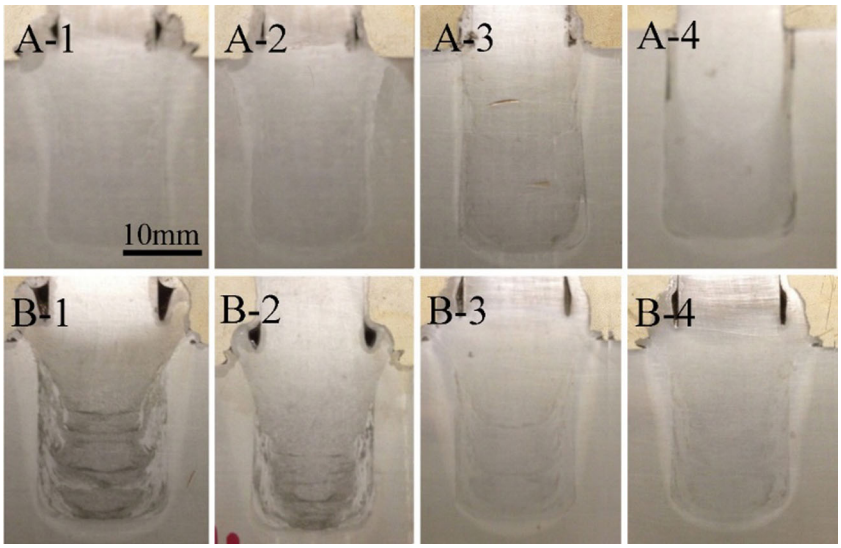


**Fig. 3** Macro observation of types A and B underwater welded joints

welded joints, the welding process can be realized in the range of 25~35 kN axial force with a rotational speed of 7000 rpm. When the axial force reached 40 kN or above, peak torque of the welding process reached the hydraulic motor maximum output torque 150 Nm (as shown in Fig. 7 A curve), thus resulting in the welding process stalling owing to overload. Observing type A welded joints macro morphology, lack of bonding defects are found at the bottom of the plug hole chamfered and initial side wall. Higher magnifications for this kind of defects are shown in Fig.4a, b. Lack of bonding in a FTP weld is in fact the initial interface between the blind hole and plug which has not yet been bonded in the welding process. It forms likely at the bottom region where round is located. One main reason in forming lack of bonding may be of the insufficient heat generation and material flow in the beginning period of FTPW process. In type B welded joints, weld root forming and the filling quality had improved, but at the part region of initial plug hole side wall had not yet realized fully metallurgical connection.

Cross-sectioning observation results of type C and D obtained joints are shown in Fig. 5 and welding peak torque are drawn in Fig. 7c, d curve. Compared with FTPW welding process in type A and B welded joints, peak torque in type C and D FTPW welding process decreases significantly. However, with the increasing of axial force from 25 to 40 kN, the peak torque dramatically increases. As with type A geometry welding trials, the 40 kN axial force leads to a too-high peak torque to the welding system in type D geometry welding trials, which results in the interruption of the welding process. Moreover, there still exists an obvious lack of bonding weld defects at the side wall of the hole in these two types of welded joints. The results indicate that type C and D geometric parameters applied can reduce the peak torque in a certain range, which broaden the range of welding parameters can be implemented, but the welding quality of joints have not been improved significantly.

Figure 6 presents macrostructure of type E~G obtained welded joints. In the E~G three types of welding joints in addition to E-4 joint existence, a small amount incomplete filling defect at the bottom of the hole, other joints were not found formation of defects. Moreover, as shown in Fig. 7 E~G curve, the peak torque could be reduced to the range of 60~90 Nm by using tapered plug rod and hole combination, and the growth rate of the peak torque also decreases with the increase of welding pressure. Comparing E~G curve in Fig. 7, it is found that the change of hole cone angles at 18°~24° range do not produce significant effect on peak torque. This suggests that the welding parameters can be adjusted in a large range to type E~G plug and hole design, which improve the adaptability of FTPW process.

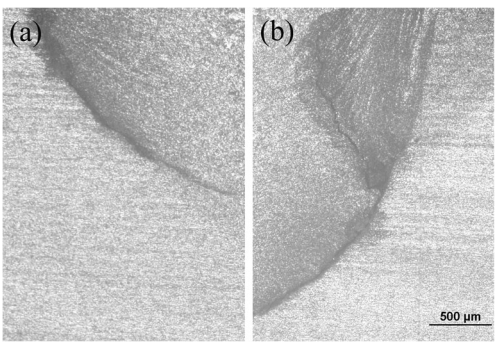


**Fig. 4** Typical welding defects in underwater FTPW weld: lack of bonding defect at weld root

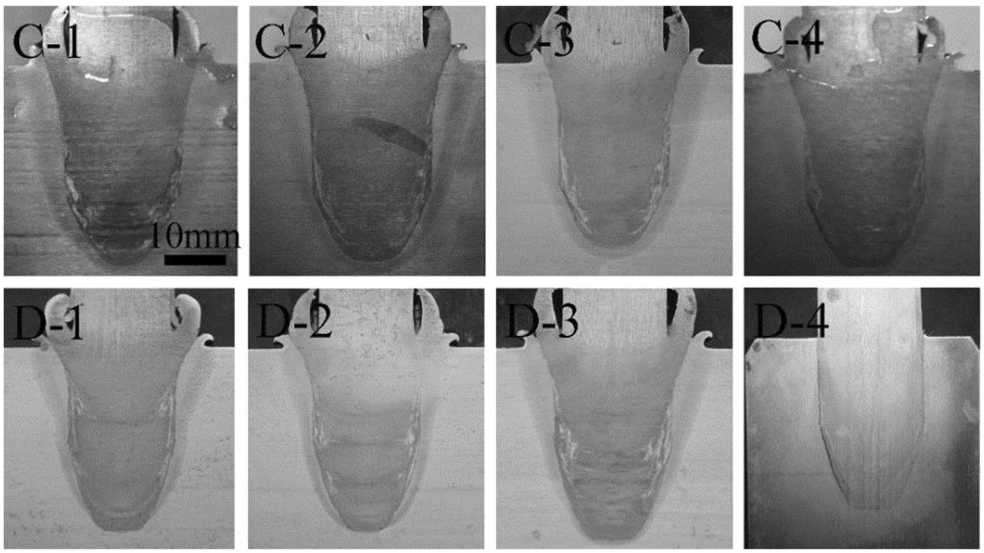


**Fig. 5** Macro observation of types C and D underwater FTPW welds

### 3.2 Macro observations for different welding parameters

The type G hole and plug was selected particularly to further expand the scope of the welding parameters. Cross-sectioning observation results of all the obtained joints are shown in Fig. 8. In most of the welding conditions when the rotational speed is equal or higher than 7000 rpm a lot of sound welds could be obtained, but lack of bonding defects are observed in the welds mostly in lower rotational speed of 6500 rpm. From the experimental results, it can be proposed that, in such hole and plug design, defect-free welds can be extensively obtained in underwater wet condition without any additional measures.

The welding process window for FTPW DH36 steel in underwater wet condition based on the present study is shown in Fig. 9. It is found that at the condition when axial force lower than 20 kN is used, the welding process cannot be performed owing to combination action of insufficient weld energy input and rapid cooling rate of water medium. Proper

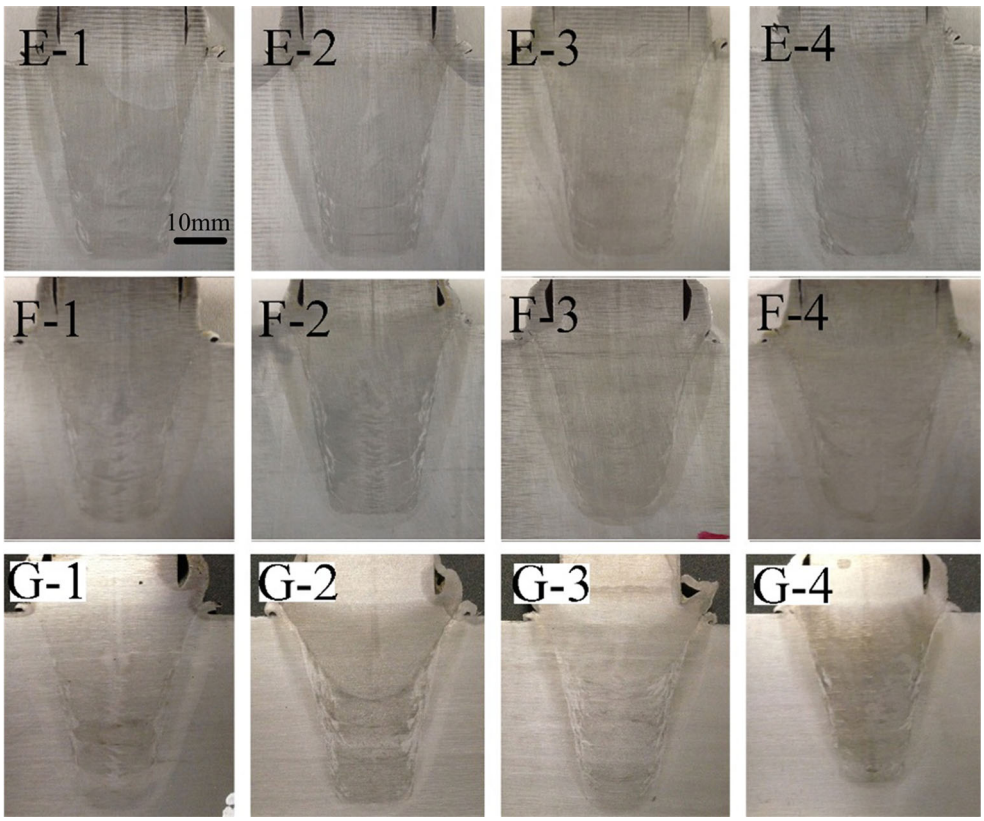


**Fig. 6** Macro observation of types E, F, and G underwater FTPW welds

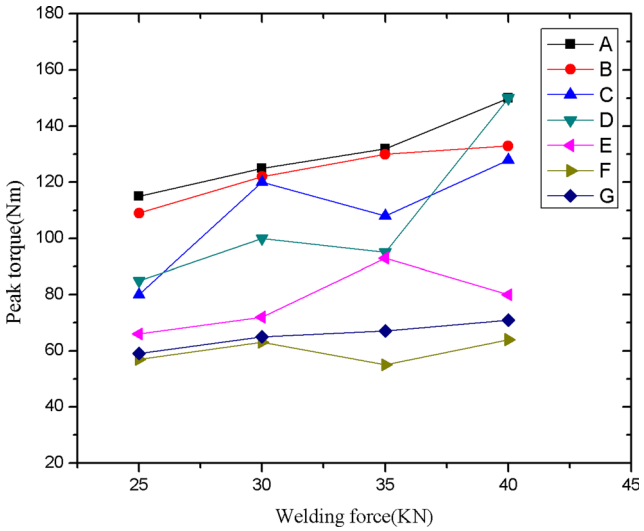


**Fig. 7** Variation of peak torque with the variation of welding force in different geometry parameters of the hole and plug

welding parameters for underwater FTPW are confirmed as the rotational speed ranging from 7000 to 7500 rpm and the welding force in the range of 30~45 kN. At relatively low rotational speed of 6500 rpm, obvious lack of bonding defects are found in most of the joints (Samples M~Q). Moreover, when a combination parameter of 6500 rpm rotational speed and 50 kN welding force is used, the welding system stalls owing to the overload of the hydraulic motor. So the result for Sample R is missed.

### 3.3 Microstructures

The overall morphology of a FTP weld can be divided into four regions according to the inhomogeneity of observations: base metal (BM), filled zone or weld metal zone (WM) forms from deposited plug materials, heat affect zone (HAZ), and flashes form from both plug materials and forged BM. Between the WM and BM, there is a distinct dark line which is traditionally named bonding line (BL) in friction welds [19, 20]. Observing the microstructure near BL (Fig. 10a, b), it is found that several fine equiaxed ferrite grains form along the initial side wall of the blind hole. These fine grains comprise a fine grain belt (FGB). The FGB is of nearly 60 μm in width and is distributed at the plug side along BL. The SEM observation (Fig. 10b) proves that the metallurgical bonding behavior could be performed by means of the nucleation of ferrite grains at the inner wall of the blind hole. As shown in Fig.10c, the EBSD map indicates that the ferrite grains in FGB are nearly equiaxed and randomly orientated, and between the units there are mostly high-angle grain boundaries. However, at

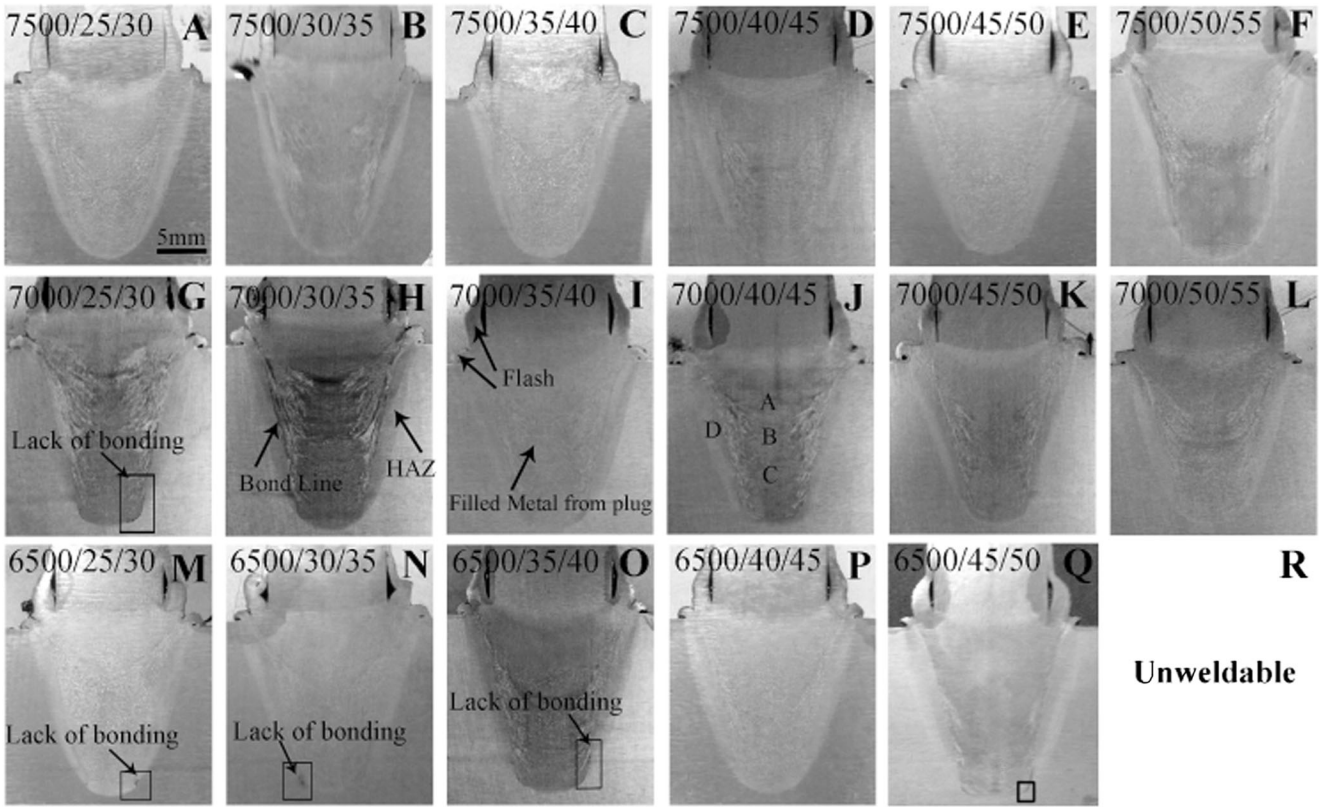


**Fig. 8** Cross-sections of weld samples for all the successful welding conditions with type G hole and plug

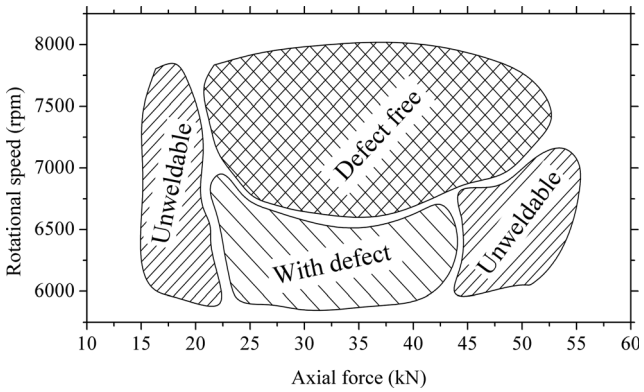


**Fig. 9** Process window for FTPW of DH36 steel in underwater wet condition when selecting type G hole and plug

the two sides of FGB where HAZ and WM are located, lathy microstructures with obvious preferred orientations are obtained.

Four typical areas marked as A, B, C, and D in Sample J were selected to investigating the microstructure evolution throughout the weld. The OM observations of regions A~D are shown in Figs. 11a~d respectively. It can be observed that in the four regions, lath-like structures dominated. Along the length direction of WM where region A (upper region of WM), B (middle region of WM), and C (lower region of WM) are located, the lathy microstructure exhibits different features. However, the microstructure of region D (HAZ) is similar to that of region C.

Further, TEM observations on such regions of A~D are shown in Fig. 12. As shown in Fig. 12a, the lath-like structure in region A is identified as lath martensite with rare carbides and some dislocations. In region B, as revealed in Fig. 12b, both upper bainite with carbides or carbon-enriched retained austenite grains between bainite ferrite laths and lath martensite can be observed. In region C, whose TEM microstructure is shown in Fig. 12c, the upper bainite is characterized with a sheave that contains several bainite laths that nucleate at the boundary of prior austenite and grows parallel to each other in the coarse prior austenite grain. As shown in Fig. 12d, the microstructure of HAZ in the weld is similar to region C in WM where several bainite laths could also be found.

Figure 13 reveals the band-contrast image and EBSD orientation map of different regions on the weld. As shown in Fig. 13a, the martensite laths would compose several blocks or packets. Between different packets, there are seemingly several high-angle boundaries of prior austenite grains. And the martensite laths were mostly separated by low-angle boundaries. In Fig. 13b, where the mixed bainite and martensite are observed, the distinction for the two kinds of lathy microstructures could be found hardly in both band contrast and EBSD patterns. Figure 13c, d present EBSD map of regions C and D which have similar microstructures mainly of bainite. In these two regions, several small sheaves containing bainite laths parallel to each other can be observed. However, the size for both sheave and bainite lath in regions C and D is finer compared with region B.

### 3.4 Mechanical properties

The hardness distribution throughout the cross-section of the weld zone (test on Sample J) is shown in Fig. 14. It exhibits a good match to the macro observations. The $HV_{10}$ cloud map outlining the weld zone where HAZ, WM, FGB, and BM are

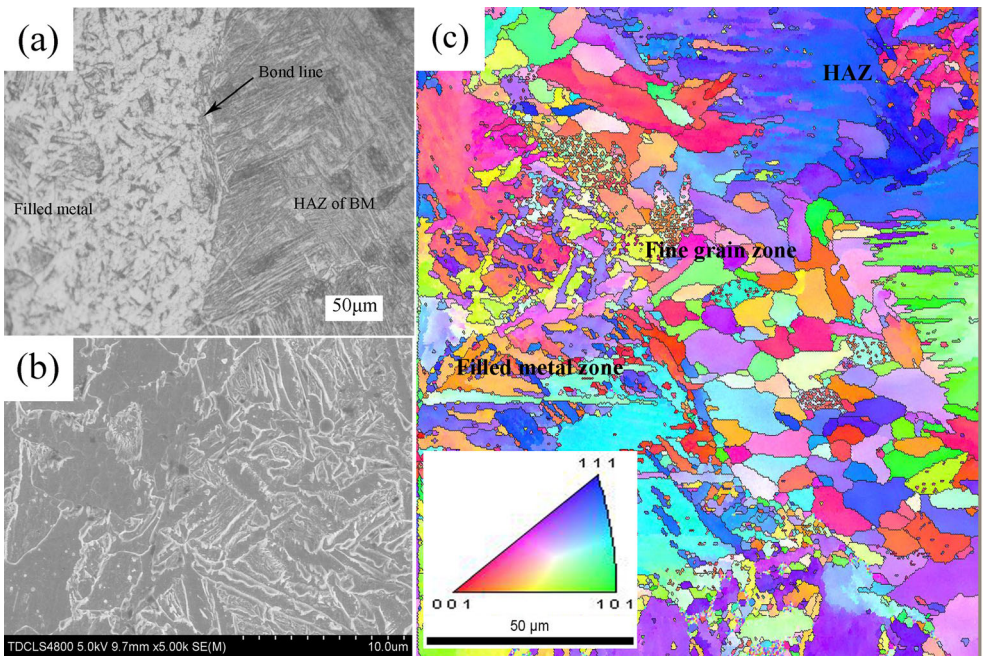


**Fig. 10** Microstructures of bond line in FTP welds: **a** OM microstructures, **b** SEM microstructures, and **c** EBSD pattern

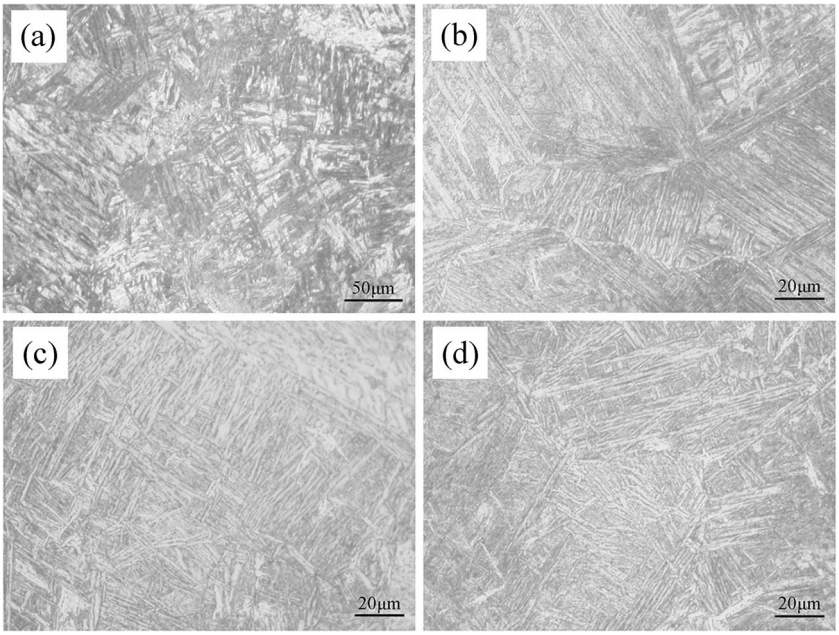


**Fig. 11** OM microstructures in different regions of the weld 4 % nital etched: **a~d** are the regions marked A~D in Sample J as shown in Fig. 8

included depicts the inhomogeneity of weld microstructures. In HAZ, the hardness value ranged from 200 to 280 $HV_{10}$, and going far away from BL to BM in horizontal direction, a decrease tendency could be observed. However, in WM, the hardness distribution seems more complicated. To the region in WM adjacent to BL, where FGB is observed, the hardness values are found in the range of 281~325 $HV_{10}$. Getting closer in horizontal direction to the weld center line, the hardness would increase significantly up to 450 $HV_{10}$ or higher. The highest hardness value is found in the upper location of WM as the region marked in Fig. 11a where the highest value of nearly 500 $HV_{10}$ is reached. In the middle and lower regions of WM, most of the testing points are of nearly 360~420 $HV_{10}$.

Tensile and impact test results indicate that the underwater wet FTPW joints would perform acceptable mechanical properties in most of the welding conditions. As shown in Fig. 15a, b, in relatively high rotational speed of 7000or

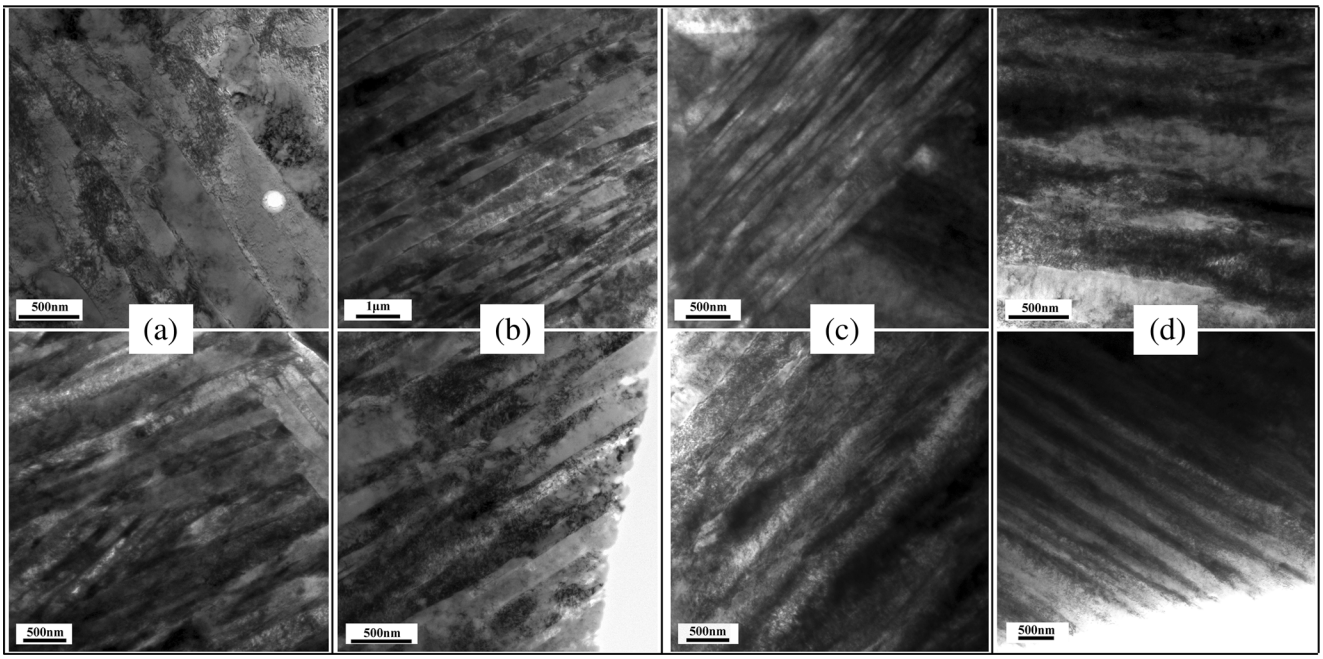


**Fig. 12** TEM microstructures in different regions of the weld : **a~d** are the regions marked A~D in Sample J as shown in Fig. 8 of which the OM microstructures are shown in Fig. 11

7500 rpm of which defect-free welds are extensively obtained, the ultimate tensile strength (UTS) for most of the samples would reach the range of 450~530 MPa. The best tensile property is found on Sample D whose UTS (535.6 MPa) and elongation (22.5 %) are nearly equal to BM owing to BM fracture mode during tensile test. However, the UTS of samples welded with 6500 rpm rotational speed exhibit poor tensile properties ranging from 320 to 421 MPa.

Figure 15c shows the 0 °C Charpy impact test results on samples V-notched at BL. For all the samples, cracking occurs and propagates along the path of BL. In defect-free welds welded with the parameters of 7000~7500 rpm rotational speed and 30~45 kN axial force, most of the V-notch impact energies could match the requirement for Class B Welds in AWS D3.6 Underwater Welding Code where 19 J, the lowest, and 27 J, the average are needed. The highest value of 42.5 J impact absorbed energy is obtained on Sample D that also has good tensile property with the same level of the BM.

## 4 Discussion

From macro morphology results as shown in Fig. 3, 5, and 6, compared with the cylindrical plug rod and hole, the tapered

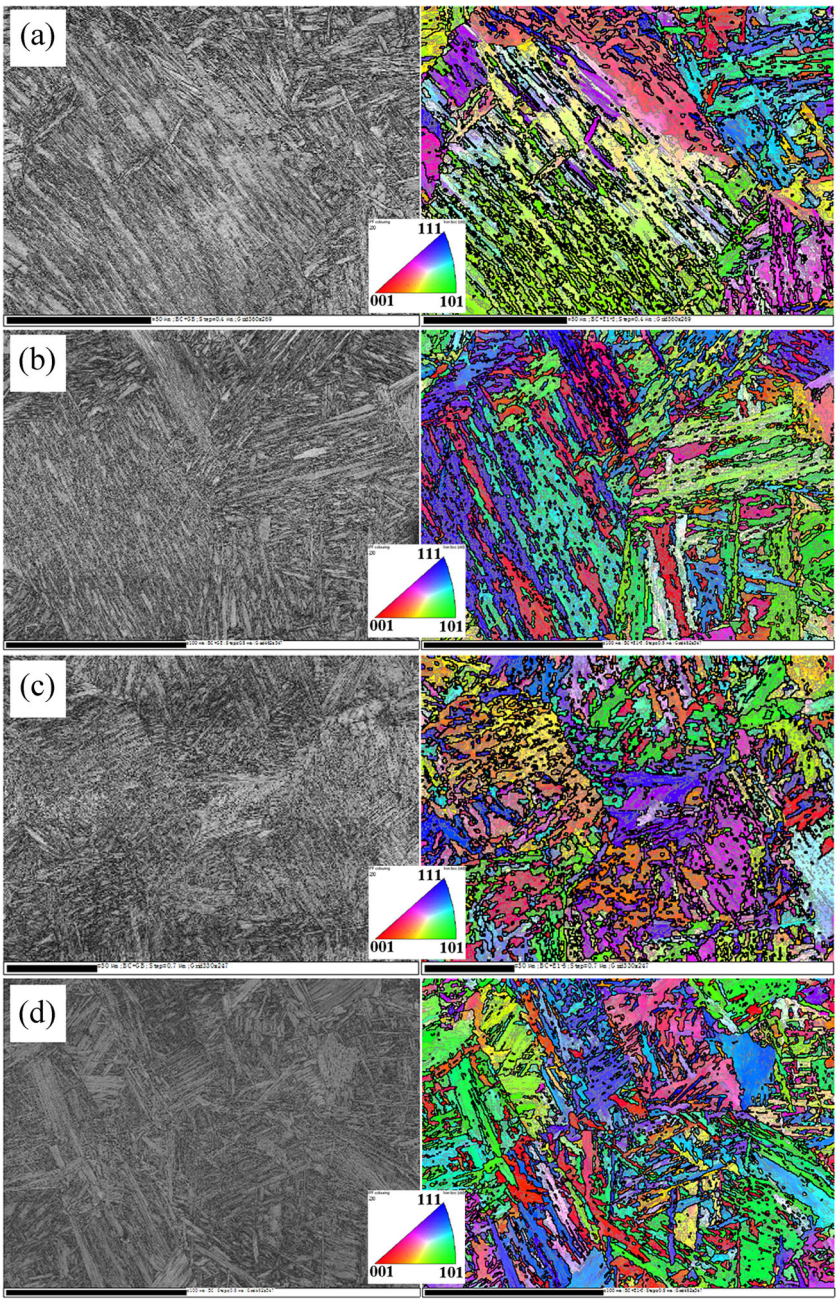


**Fig. 13** Band contrast image and EBSD orientation map for different regions in the weld: **a~d** are the regions marked A~D in Sample J as shown in Fig. 8 of which the OM microstructures are shown in Fig. 11

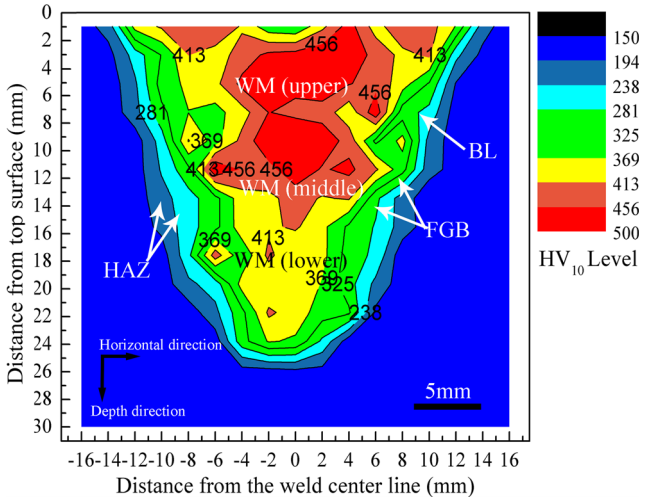


**Fig. 14** Typical hardness distribution feature through the cross-section of underwater FTPW joint

hole and plug combination often exhibit better welded joints quality. This is attributed to the conical surface under axial force that not only increases the contact area of the plug and hole but can also provide the radial force, resulting in producing more friction heat and being beneficial to the plastic flow of materials [11, 21]. However, the tapered plug and hole must have good fitting dimensions to ensure the contact surface and the bottom hole gap owning plenty of thermoplastic materials with good fluidity. Moreover, as the welding trials conducted in underwater wet condition, plug hole bottom area with the welding process proceeding should be able to exclude internal water, to prevent the residual bubbles in the welded joints, which affects the welding quality. If the plug cone angle is too small, there is no obvious difference with cylindrical plug rod. But if the plug cone angle is too big, a larger diameter plug is needed, which is beyond the bearing capacity of the equipment. Besides, as shown in Fig. 7, tapered plug and hole could reduce the peak torque into a suitable range, thus broadening the range of welding parameters can be implemented. Based on our present research results, suitable geometry parameters are obtained, that is : the hole cone angles change at 18°~24° range, and the plug cone angles are slightly smaller than the hole cone angles of 2°~3° .

Based on the cross-sectioning results as shown in Fig. 8, it can be proposed that the FTPW process certainly has the potential use for repairing and welding steel in underwater wet conditions. The possible parameters for high-quality welds are seemingly of rotational speed up to 7000 rpm and axial force

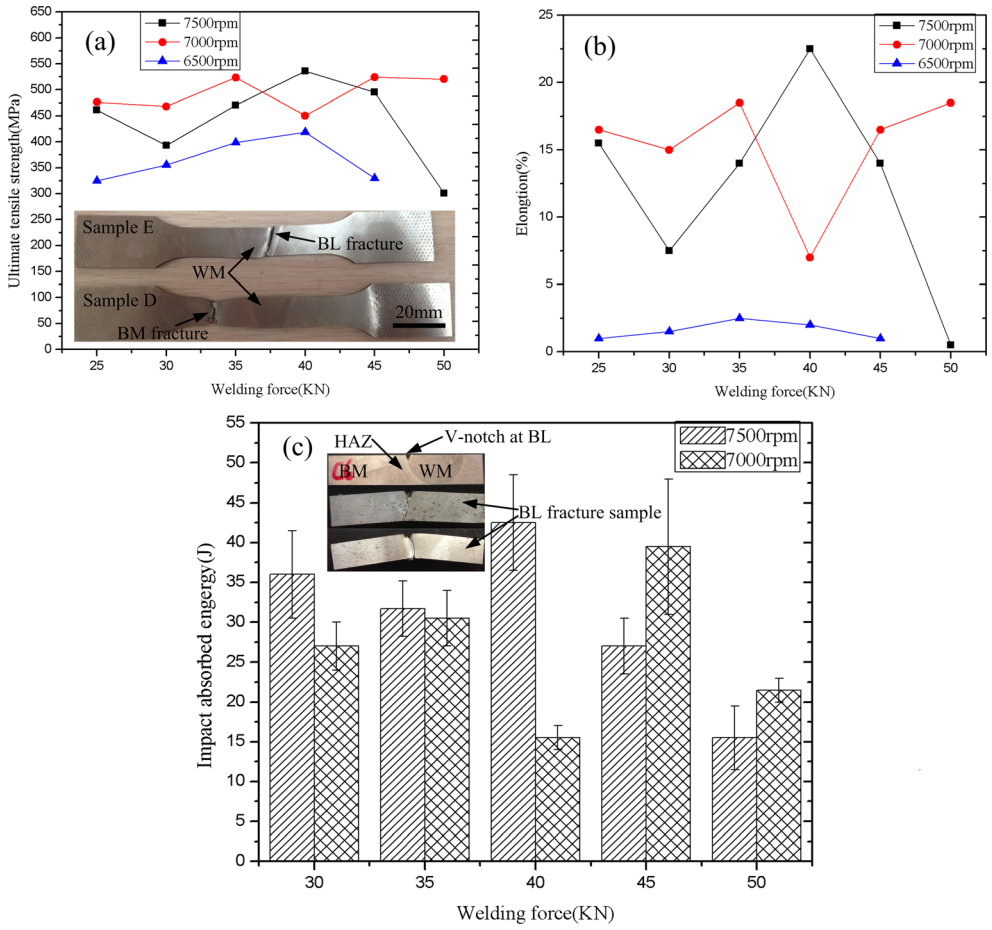


**Fig. 15** **a** The ultimate tensile strength, **b** elongation, and **c** bond line impact absorbed energy for underwater FTPW joints. Details are illustrated in Table 3

ranged in 30~45 kN. When a rotational speed lower than 6500 rpm is used, lack of bonding defects are likely to form in the inner weld. When a too-low axial force (20 kN or lower) is used, a balance of water cooling and frictional heat generation would be achieved owing to the insufficient welding energy input. In this balance situation, the frictional heat could not transfer up to the plug any further, therefore the blind hole fails to be fully filled. However, a too-high axial force (higher than 50 kN) would cause the FTPW process to be stalled owing to the overload of the welding power system.

Observation of microstructural evolutions indicates that the microstructure for underwater FTP weld is mainly of lath structures, but exhibits heterogeneous features (Figs. 11, 12, and 13). This characteristic can also be reflected on the hardness distribution map. In the upper region of WM (region A in Sample J), the microstructure consists of several martensite laths which form by both water quenching and forging effects of the plug material. The upper WM has the highest hardness on the weld cross-section (Fig. 14) whose values are ranged from 450~500 $HV_{10}$. In middle WM, where mixed microstructures of bainite and martensite can be found, the hardness decreases to nearly 400 $HV_{10}$ owing to the decreasing amount of martensite. In lower WM, a further decrease of hardness lower than 360 $HV_{10}$ is observed. That is mainly caused by the disappearance of martensite in this region, but a large amount of bainite instead. It should be noted that although similar microstructures of bainite are found in both HAZ and lower WM, the strength of these two exhibits different levels. The much higher hardness in lower WM than HAZ may be caused by forging action from axial load during the welding process.

Metallurgical bonding between the initial hole sidewall and plug material may be identified as the formation of new grain boundaries (as shown in Fig. 10) by means of the combination action from stress and heat at the welding interface. In welding process, some of the equiaxed fine ferrite grains would form along the hole sidewall. These ferrite grains that surrounded the filled plug material compose a belt-like structure along the hole inner sidewall.

Except for Sample D, all the tensile samples were fracture at bonding line during tensile test. This indicates that, in most of the conditions, the bonding strength at initial interface is lower than the tensile strength of the base metal. But for defect-free welds with relatively high rotational speed of 7000 rpm or 7500 rpm, the FTPW joints have favorable tensile properties,where the ultimate tensile strength (UTS) for most of the samples would reach the range of 450~530 MPa. Besides, the BL V-notched fracture samples were all fractured along the BL path and exhibit much lower impact absorbed energies. This is mainly affected by the coarsening of the austenite grains, the formation of coarse bainite and martensite laths with obvious preferred orientations and local stress concentration [17].

## 5 Conclusions

In this study, the influence of geometry and welding parameters on the quality of DH36 marine steel FTP welded joints underwater were investigated. The following conclusions could be drawn:

(1) Tapered holes and plugs with the hole cone angles changing at 18°~24° range, and the plug cone angles slightly smaller than the hole cone angles of 2°~3° can greatly improve the quality of underwater welding joints and welding process stability.
(2) Defect-free welds could be obtained vastly by FTPW in underwater wet condition without any protection measures. The optimized parameters are rotating speed higher than 7000 rpm and axial force ranged from 30~45 kN.
(3) Metallurgical bonding between the hole and plug is performed by means of ferrite nucleation at the sidewall of the blind hole. The microstructure in weld zone would involve upper and lower bainite, equiaxed ferrite, and lath martensite.
(4) The hardness distribution cloud map indicates heterogeneous microstructure features of the weld zone. From upper WM to lower WM, the hardness decreases from 500 $HV_{10}$ to 360 $HV_{10}$.
(5) FTPW joint welded with 7500 rpm and 40 kN exhibits 535.6 MPa ultimate tensile strength, 22.5 % elongation, and 42.5 J impact energy at BL (0 °C).

**Acknowledgment** This research work was financially supported by National Natural Science Foundation of China (51475327). Great thanks are given to Jun Cao and Wei Xu from Offshore Oil Engineering Co., LTD of China for supporting the experiment.

## References

1. Fydrych D, Rogalski G, Łabanowski J (2014) Problems of underwater welding of higher-strength low alloy steels. Institute of Welding Bulletin 5
2. Łabanowski J, Fydrych D, Rogalski G (2008) Underwater welding—a review. Adv Mater Sci 8(3):11–22
3. Pessoa ECP, Bracarense AQ, Dos Santos VR, Monteiro M, Vieira LA, Marinho RR Challenges to develop an underwater wet welding electrode for "class A welds" classification, as required in the AWS D3. 6 code. In: ASM Proceedings of the International Conference: Trends in Welding Research, 2013. p 259.
4. Chen B, Tan C, Feng J (2015) A study on the arc characteristics of underwater wet welding process. Int J Adv Manuf Technol. doi: 10.1007/s00170-015-8159-y
5. Meyer A, Pauly D, Santos JFD, Pinheiro G, Roos A, Gibson D, G.R. (June 3, 2001–June 8, 2001) 20th International Conference on Offshore Mechanics and Arctic Engineering. American Society of Mechanical Engineers: pp. 145–151.
6. Fydrych D, Łabanowski J, Rogalski G, Haras J, Tomków J, Świerczyńska A, Jakóbczak P, Kostro Ł (2014) Weldability of

S500MC steel in underwater conditions. Adv Mater Sci 14(2):37–45
7. Yeh FWT, da Cunha PHC P, Lessa CRL, Clarke T, Strohaecker T (2013) Evaluation of discontinuities in A36 steel repairs with friction hydro pillar processing using different axial forces. ISIJ Int 53(12):2269–2271
8. Hattingh D, Van Zyl C (2012) Temperature distribution for a friction taper stud weld in thick walled 10CrMo910 steel. RDJ South Afri Inst Mech Eng 28:37–45
9. Paes M, Pope A (2009) Influence of Process Parameters in the TMAZ Microstructural Evolution of C-Mn Steels Friction Hydro-Pillar Welded Joints. In: Trends in Welding Research: Proceedings of the 8th International Conference, June 1–6, 2008, Callaway Gardens Resort, Pine Mountain. ASM International, Georgia, USA, p 381
10. Unfried SJ, Paes M, Hermenegildo T, Bastian F, Ramirez A (2010) Study of microstructural evolution of friction taper plug welded joints of C–Mn steels. Sci Technol Weld Join 15(6):506–513
11. Meyer A (2003) Friction hydro pillar processing-bonding mechanism and properties. Fakultät für Maschinenbau und Eletrotechnik der TechnischenUniversität Carolo-Wilhelmina zu Braunschweig
12. Ambroziak A, Gul B (2007) Investigations of underwater FHPP for welding steel overlap joints. Arch Civil Mech Eng 7(2):67–76
13. Hattingh D, Bulbring D, Els-Botes A, James M (2011) Process parameter influence on performance of friction taper stud welds in AISI 4140 steel. Mater Des 32(6):3421–3430
14. Cui L, Yang X, Wang D, Cao J, Xu W (2014) Experimental study of friction taper plug welding for low alloy structure steel: welding process, defects, microstructures and mechanical properties. Mater Des 62:271–281
15. Chludzinski M, Paes M, Bastian F, Strohaecker T (2012) Fracture toughness of friction hydro-pillar processing welding in C–Mn steel. Mater Des 33:340–344
16. Yin Y, Yang X, Cui L, Cao J, Xu W (2015) Investigation on welding parameters and bonding characteristics of underwater wet friction taper plug welding for pipeline steel. Int J Adv Manuf Technol:1–11
17. Cui L, Yang X, Wang D, Hou X, Cao J, Xu W (2014) Friction taper plug welding for S355 steel in underwater wet conditions: welding performance, microstructures and mechanical properties. Mater Sci Eng A 611:15–28
18. AWS D3.6M (2010) 2010 Underwater welding code.
19. Bhamji I, Preuss M, Threadgill P, Addison A (2011) Solid state joining of metals by linear friction welding: a literature review. Mater Sci Eng 27(1):2–12
20. Damodaram R, Raman SGS, Rao KP (2013) Microstructure and mechanical properties of friction welded alloy 718. Mater Sci Eng A 560:781–786
21. Xu Y, Jing H, Han Y, Xu L (2015) Numerical simulation of the effects of various stud and hole configurations on friction hydro-pillar processing. Int J Mech Sci 90:44–52